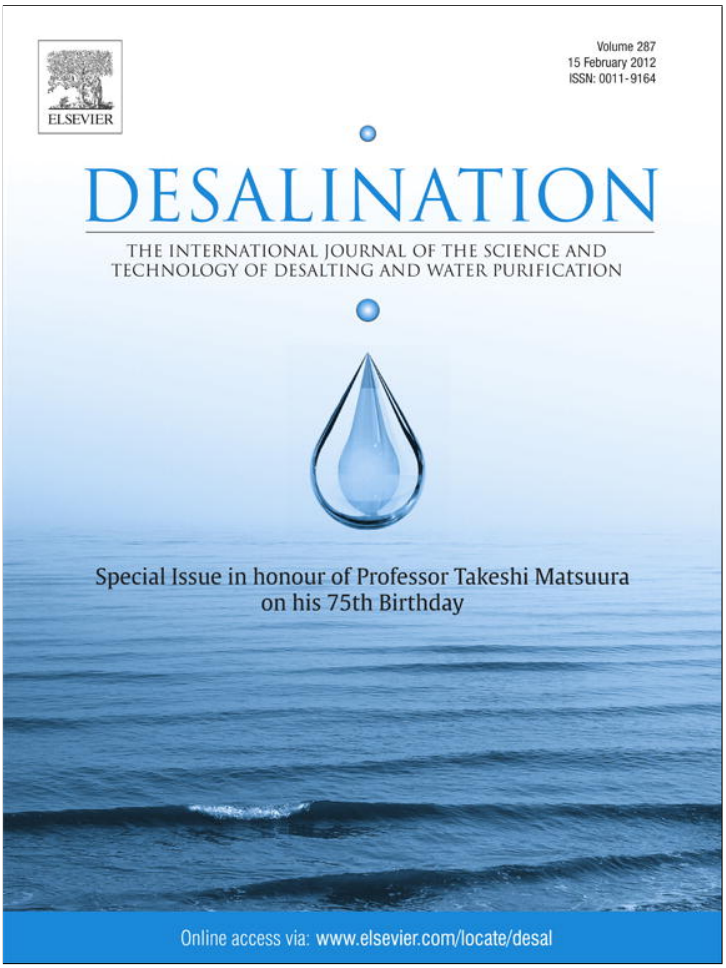

Desalination 287 (2012) 340–349

Contents lists available at SciVerse ScienceDirect

Desalination

journal homepage: www.elsevier.com/locate/desal

# Impacts of operating conditions and solution chemistry on osmotic membrane structure and performance

Mavis C.Y. Wong, Kristina Martinez, Guy Z. Ramon [1], Eric M.V. Hoek *

*Department of Civil and Environmental Engineering and California NanoSystems Institute, University of California, Los Angeles, CA, USA*

ARTICLE INFO

*Article history:*
Received 20 June 2011
Received in revised form 11 October 2011
Accepted 13 October 2011
Available online 17 November 2011

*Keywords:*
Forward osmosis
Membrane structural parameter
Concentration polarization
Cellulose triacetate

ABSTRACT

Herein, we report on changes in the performance of a commercial cellulose triacetate (CTA) membrane, imparted by varied operating conditions and solution chemistries. Changes to feed and draw solution flow rate did not significantly alter the CTA membrane's water permeability, salt permeability, or membrane structural parameter when operated with the membrane skin layer facing the draw solution (PRO-mode). However, water and salt permeability increased with increasing feed or draw solution temperature, while the membrane structural parameter decreased with increasing draw solution, possibly due to changes in polymer intermolecular interactions. High ionic strength draw solutions may de-swell the CTA membrane via charge neutralization, which resulted in lower water permeability, higher salt permeability, and lower structural parameter. This observed trend was further exacerbated by the presence of divalent cations which tends to swell the polymer to a greater extent. Finally, the calculated CTA membrane's structural parameter was lower and less sensitive to external factors when operated in PRO-mode, but highly sensitive to the same factors when the skin layer faced the feed solution (FO-mode), presumably due to swelling/de-swelling of the saturated porous substructure by the draw solution. This is a first attempt aimed at systematically evaluating the changes in performance of the CTA membrane due to operating conditions and solution chemistry, shedding new insight into the possible advantages and disadvantages of this material in certain applications.



## 1. Introduction

The amount of accessible fresh water in the world is estimated to be less than 1% of the Earth's entire water supply, whereas nearly 70% of the planet is covered with ocean water [1,2]. With a rapidly expanding global population, fresh water is becoming a scarce resource and hence, there is growing interest in the use of desalination technology to produce fresh water from ocean water as well as other non-traditional water sources such as brackish and waste-water. The most popular commercial technologies for desalination include thermal processes (multi-stage flash distillation, multi-effect distillation, mechanical vapor compression, etc.) and membrane processes (reverse osmosis, nanofiltration, and electro-dialysis) [3]; the relative merits and limitations of these are well studied [4]. While not a new idea, forward osmosis (FO) is emerging as a possible future alternative to these conventional desalting technologies, and FO is considered one of "three technologies [that] promise to reduce the energy requirements of desalination by up to 30 percent" [5].

Forward osmosis is the transport of water through a semi-permeable membrane from a relatively low concentration solution (feed) to a relatively high concentration solution (draw), that is, from a high to low water chemical potential. Recently, engineered-osmosis membrane processes have been receiving increased attention due to their significantly lower operating pressures and lower fouling propensity. Therefore, FO may be developed into a relatively low energy and low cost desalination process [6,7]. Engineered-osmosis membrane processes are also being developed for wastewater reclamation [8,9], food and pharmaceutical concentration [10,11], as well as renewable energy production from salinity gradients [12–15].

During the osmotic transport, water permeation across the membrane from the feed solution dilutes the draw solution concentration at the membrane surface, while a small amount of salt diffuses through the membrane from the draw to concentrate the feed as membranes are not completely impermeable to salt. This reduction in the effective trans-membrane salinity difference, or the osmotic pressure difference, is referred to as external concentration polarization (ECP). The effect of ECP can generally be minimized by increasing the mass transfer rates in the feed and draw flow channels [9].

Commercially available semi-permeable osmotic membranes have an asymmetric structure comprised of a thin, dense skin layer where

* Corresponding author at: University of California, Los Angeles, 5732-G Boelter Hall, P.O. Box 951593, Los Angeles, CA, 90095-1593, USA. Tel.: +1 310 206 3735; fax: +1 310 206 2222.
*E-mail address:* emvhoek@ucla.edu (E.M.V. Hoek).
[1] Present address: Department of Mechanical and Aerospace Engineering, Princeton University, Princeton, NJ 08544, USA.

0011-9164/$ – see front matter © 2011 Elsevier B.V. All rights reserved.
doi:10.1016/j.desal.2011.10.013

salt rejection occurs formed over a porous substructure, which provides mechanical support. In what follows, experiments performed with the membrane skin layer facing the draw solution will be referred to as PRO-mode while those performed with the membrane skin layer facing the feed solution will be referred to as FO-mode. The two modes of operation are used in the FO experiments investigated herein. When operated in PRO-mode, solute permeating through the skin layer concentrates the feed solution, and the porous support creates a stagnant zone where solute is transported solely by hindered diffusion, exacerbating the reduction in the effective osmotic pressure difference, resulting in concentrative internal concentration polarization (ICP) (Fig. 1a). Dilutive ICP occurs when operating in FO-mode when water permeating through the membrane dilutes the draw solution within the porous support where, again, solute mass transfer is slow. Both cases of ICP result in a substantial reduction of the effective osmotic pressure difference across the active layer of the membrane (Fig. 1b), which in turn lowers the water flux across the membrane. Furthermore, since the polarization occurs within the porous membrane support, it cannot be reduced by hydrodynamic means, e.g. through an increased cross-flow velocity [9,16,17].

Consequently, a great deal of effort has been extended towards understanding and quantifying ICP. These studies have mostly been aimed at estimating the resistance to mass transfer within the porous support. The structural parameter has been used to reflect the combined effects of porous substructure porosity, tortuosity and thickness, with the foregone conclusion that a porous, thin support with straight pores is essential for minimizing ICP. An implicit assumption has been that the structure of the membrane support is constant and is not affected by operating conditions. This is indeed plausible if the porous material is completely inert; in practice, however, the polymeric material may interact, to various extents, with the solution as changes in temperature and chemical composition are made. For example, hydrogel polymers have been reported to absorb water and swell [18,19], increasing its volume and mass significantly. Cellulosic polymers have also been found to swell in the presence of various mixtures [20–23]. Furthermore, cellulosic polymers contain hydroxyl groups [24,25] that could interact electrostatically with polar solvents and ionic solutions. Thus, there may be inherent changes to membrane structure and performance as a result of the interaction between polymeric membranes and the solution it is in contact with.

Little effort has thus far been extended towards understanding the possible effect of solution–membrane interactions on the structural mass transfer resistance of the porous support. The increased water flux with increasing temperature observed in RO has long been known (e.g. [26]), but this has not, to the best of our knowledge, been investigated for FO where two streams contact the membrane on either side. Recently, Achilli et al. [6] reported that different salts producing the same osmotic pressure did not have a significant effect on the calculated structural parameter for the CTA membrane in FO-mode. Indeed, the variation over the entire data range amounted to less than 20%. However, at closer scrutiny it does seem that larger variations may exist within the separate data for the varying salts used. Furthermore, it is interesting to note that the average value reported for the CTA membrane, 470 μm, is much lower than ~670 μm, reported in another study with the membrane in PRO-mode [17] and in yet another study, the structural parameter was reported to vary between 500 and 700 μm [18]. Certainly, this reported variability warrants further scrutiny to determine whether different testing conditions could induce such differences in the structural parameter of the CTA membrane.

The purpose of this study was to determine how and to what extent FO process conditions affect the water flux across the membrane. Specifically, what changes are observed for the water permeability and calculated structural parameter with variations in solution flow rate, temperature, composition, and membrane orientation (see Table 1 for the matrix of experimental conditions investigated herein). In order to systematically understand the effect of process conditions, a commercial FO membrane was first characterized through RO experiments, followed by FO experiments through which possible changes to the membrane structure were investigated.

## 2. Materials and methods

### 2.1. Membrane

The FO membrane used is a commercially available cellulose triacetate (CTA) membrane (Hydration Technologies Innovations, Albany, OR), which is an asymmetric and a moderately hydrophilic membrane [25]. By appearance, the skin layer side of the membrane is

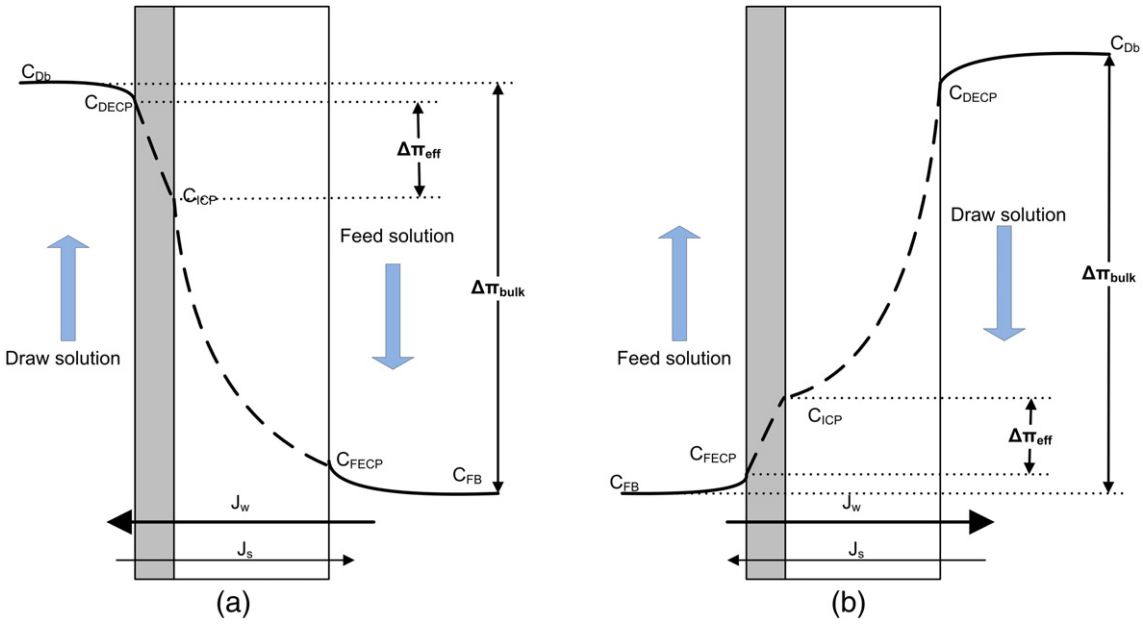


**Fig. 1.** Concentration polarization in osmotic membrane processes. The reduced concentration at the external membrane surfaces is due to external CP. Concentrative internal CP (a) occurs when the skin layer faces the draw, and salt builds up in the porous support (PRO-mode), whereas dilutive internal CP (b) occurs when the skin layer faces the feed, and water flux dilutes the draw concentration (FO-mode).

**Table 1**
Matrix of experiments and conditions.

| Conditions | | Varying flow rates | Varying temperatures | Varying concentration | Varying solution composition | Varying membrane orientation |
|---|---|---|---|---|---|---|
| Temperature (°C) | | 20 | 10, 20, 30 | 20 | | |
| Flow rates (gpm) | Draw | 0.05, 0.10, 0.15 | | 0.10 | | |
| | Feed | 0.05, 0.10, 0.15 | | 0.10 | | |
| Draw solution concentration (g/L) and composition | | 32 NaCl | 32 NaCl | 10, 32, 50, 70 NaCl | 32 NaCl<br>32 MgSO4<br>32 Instant Ocean | 32 NaCl<br>32 MgSO4<br>32 Instant Ocean |
| Feed solution | | | | Deionized water | | |
| Operating mode[a] | | | | PRO | | FO |

[a] PRO-mode: membrane skin layer faces draw solution; FO-mode: membrane skin layer faces feed solution.

more lustrous and smooth than the dull support layer side. The membrane is kept in deionized water at 4 °C before use to avoid irreversible shrinking upon drying. SEM images of the membrane [6,27] have shown that the membrane is a thin polymer film supported by a woven polyester mesh embedded in polymer substrate. For the majority of the experiments, the membrane was tested in PRO-mode. Additional experiments were conducted in FO-mode in order to comparatively probe the different effects of ICP under each membrane orientation.

### 2.2. Characterization of membrane transport coefficients

The FO membrane's water and salt permeability were determined through experiments in RO mode. The RO system employed is a cross-flow system consisting of six stainless steel cells operating under the same pressure and the same feed water (Fig. S1). Each cell has an effective membrane area of 19 $cm^2$ and a channel height of 2 mm. The feed solution was pressurized in the system using a diaphragm pump (Hydracell; Wanner Engineering, Minneapolis, MN). The feed solution was kept at a constant temperature by heat exchanger coils, submerged in the feed tank, connected to a water chiller (NTE RTE7; Fisher Scientific, Pittsburgh, PA). The conditions for these RO experiments were chosen to reflect those used in subsequent FO experiments. Specifically, the water flux was determined for the temperatures and solution chemistries investigated herein, as presented in Table 1.

In order to determine the intrinsic water permeability, $A$, the feed tank was filled with Milli-Q water produced from Super-Q water systems (Millipore Corp., Billerica, MA), and the permeate flow rate was measured by a digital flow meter (Optiflow 1000; Agilent Technology, Foster City, CA) at a given applied hydraulic pressure and temperature. The pure water permeability may be calculated as the slope of a pressure-flux plot, through the relation

$$A = \frac{J_w}{\Delta P}. \tag{1}$$

The solution permeability is defined here as the apparent water permeability during filtration of salt solution and, hence, accounts for concentration polarization effects. The water permeability in the presence of a salt species $i$ is as defined as:

$$A_i = \frac{J_w}{\Delta P - \Delta\pi} \tag{2}$$

where $J_w$ is the water flux through the membrane in presence of salt in the feed solution. The intrinsic salt permeability, $B$, was determined by measuring the feed and permeate conductivity with a calibrated conductivity meter (Accumet XL20, Cole Parmer, Barrington, IL) at a given pressure and feed solution chemistry, and calculated by [28, 29]

$$B = J_w\left(\frac{1-R}{R}\right)\exp\left(\frac{-J_W}{k}\right) \tag{3}$$

where $R$ is the observed solute rejection and calculated by $R = 1 - C_p/C_f$ in which $C_p$ is the permeate solute concentration and $C_f$ is the feed solute concentration. The mass transfer coefficient, $k$, is dependent on the cross-flow velocity, the channel geometry and solution properties, and may be calculated using mass transfer correlations. While several such correlations may be found in the literature for spacer-filled channels (for example, [30–32]), the following correlation proposed by Guillen et al. was chosen since it has been specifically developed for the experimental flow-cell employed [23],

$$Sh = 0.46(ReSc)^{0.36} = \frac{kd_H}{D} \tag{4}$$

in which $Sh$ is the Sherwood number, $Re = (u_0\rho d_H)/\mu$ is the Reynolds number and $Sc = \mu/(\rho D)$ is the Schmidt number, with $k$ denoting the mass transfer coefficient, $u_0$ the average velocity in the membrane channel, $d_H$ is the hydraulic diameter, $D$ is the diffusion coefficient, $\mu$ is the viscosity and $\rho$ the density.

The density and viscosity of the salt solutions were determined by correlations found in the literature [33,34]. The diffusion coefficient of the solute in water is calculated using the correlations developed by [35], and corrected for temperature differences using the Stokes–Einstein law of diffusion [36]. However, due to the complex composition of Instant Ocean, the diffusivity could only be determined approximately from weighted averages. The calculated solution properties are presented in Table 2.

### 2.3. Forward osmosis experiments

The FO experiments were conducted using a custom designed flow cell made of polycarbonate. The flow channels on both sides of the membrane are 2.54 cm wide, 7.62 cm long and 1 mm high. The draw solution flowed counter-currently to the feed solution, controlled independently by gear pumps (MicroPump A, Cole Parmer, Barrington, IL). The solution flow rates were measured by rotameters (Blue White Industries Ltd, Huntington Beach, CA). The temperature of the solutions were kept constant with immersed stainless steel cooling coils (JFD Tube & Coil Products, Inc, Hamden, CT) connected to re-circulating water baths with temperature controls (NESLAB RTE-7, Thermo Fisher Scientific Inc, Waltham, MA). The temperature of the solutions for different experiments varied from 10 to 30 °C to simulate seawater conditions. The draw solution was kept on a balance (PI-2002, Denver Instruments, Bohemia, NY) with the mass of the draw solution recorded every 30 s on a computer, from which the water flux is calculated. Only the first 30 min of each experiment were used for analysis; both the water flux and salt flux reached a steady-state approximately 5 min into the experiment. The initial volume of both draw and feed solutions is one liter, and after 30 min less than 30 mL of water has permeated through the membrane to the draw and less than 1 g of salt has passed into the feed for all experiments. Thus, within the duration of the experiment, dilution of the draw and concentration of the feed was negligible.

**Table 2**
Properties of draw solutions under experimental conditions.

| Parameter | Symbol (Units) | NaCl | | | | | | | | $MgSO_4$ | Instant Ocean |
|---|---|---|---|---|---|---|---|---|---|---|---|
| Concentration | C (g/L) | | | 32 | | | 10 | 50 | 70 | 32 | 32 |
| Bulk osmotic pressure | $\pi_{bulk}$ ($10^6$ Pa) | | | 2.74 | | | 8.41 | 4.36 | 6.20 | 0.65 | 2.55 |
| Ionic strength | I (mol/L) | | | 0.547 | | | 0.171 | 0.855 | 1.197 | 0.519 | 0.645 |
| Temperature | T (°C) | | 20 | | 10 | 30 | | | 20 | | |
| Flow rate | Q (gpm) | 0.05 | 0.10 | 0.15 | | | | 0.10 | | | |
| Water viscosity | μ ($10^{-3}$ Pa-s) | 1.03 | 1.03 | 1.03 | 1.31 | 0.789 | 1.01 | 1.06 | 1.09 | 1.15 | 1.08 |
| Water density | ρ (kg/m$^3$) | 1021 | 1021 | 1021 | 1023 | 1018 | 1007 | 1032 | 1045 | 1017 | 1024 |
| Salt diffusivity | D ($10^{-9}$ m$^2$/s) | 1.35 | 1.35 | 1.35 | 0.68 | 2.03 | 1.36 | 1.37 | 1.41 | 0.39 | 1.27 |
| Reynolds no. | – | 236 | 471 | 707 | 374 | 616 | 476 | 466 | 458 | 421 | 457 |
| Schmidt no. | – | 750 | 750 | 750 | 1889 | 382 | 737 | 748 | 739 | 969 | 781 |
| Sherwood no. | – | 36 | 46 | 53 | 59 | 40 | 46 | 45 | 45 | 48 | 46 |
| Mass transfer coefficient | k ($10^{-5}$ m/s) | 2.5 | 3.2 | 3.7 | 2.1 | 4.7 | 3.2 | 3.2 | 3.3 | 2.9 | 3.2 |

The resistance to solute diffusion by the porous substructure, $K$, depends on whether the skin layer faces the feed or the draw solution. For the skin layer facing the draw and the feed solution as Milli-Q water ($\pi_{FECP}=0$) [12,37],

$$K = \left(\frac{1}{J_W}\right)\ln\left(\frac{B + A\pi_{DECP} - J_W}{B}\right). \quad (5)$$

And, when the skin layer faces the feed,

$$K = \left(\frac{1}{J_W}\right)\ln\left(\frac{B + A\pi_{DECP}}{B + J_w}\right) \quad (6)$$

where $A$, $B$, $\pi_{DECP}$ and $J_w$ is the water permeability, salt permeability, osmotic pressure of the draw solution accounting for ECP and the water flux through the membrane, respectively. The reduction in osmotic pressure of the draw due to external concentration polarization depends on the mass transfer coefficient, $k$, and is calculated by,

$$\pi_{DECP} = \pi_D \exp\left(\frac{-J_W}{k}\right) \quad (7)$$

where the osmotic pressure is calculated by the Gibbs equation [38]. To determine how the membrane structure changes with different conditions, it is necessary to uncouple the solute resistance from the draw solution chemistry by defining a membrane structural parameter, $S$, as

$$S = KD = \frac{t_{sup}\tau}{\varepsilon}, \quad (8)$$

where $t_{sup}$, $\tau$ and $\varepsilon$ are the support membrane thickness, tortuosity and porosity, respectively [39].

### 2.4. Feed and draw solutions

For all experiments conducted, the feed solution was Milli-Q water, while the draw solutions were prepared by addition of salts to Milli-Q water. The NaCl and $MgSO_4\cdot(H_2O)_7$ used to make the draw solutions were ACS reagent-grade (Fisher Scientific, Pittsburgh, PA) and were used as received. To simulate seawater, commercial sea salt was also used to make the draw solution, which is comprised mostly of $Na^+$, $Cl^-$, $Mg^{2+}$, $SO_4^{2-}$, $K^+$, $Ca^{2+}$ and $HCO_3^-$ (Instant Ocean®, Spectrum Brands Inc., Atlanta, GA).

#### 2.4.1. Variation of solution flow rate

In order to investigate the effect of solution flow rate on water flux through the membrane, the flow rates of the draw and feed solutions were varied independently in each experiment from 0.19 L/min to 0.38 L/min to 0.57 L/min (0.05, 0.10, 0.15 gpm, respectively). The experiments were conducted in PRO-mode, with a constant draw solution concentration of 32 g/L NaCl, while both draw and feed solution temperatures are kept constant at 20 ± 1 °C.

#### 2.4.2. Variation of solution temperature

In these experiments, aimed at examining the effect of solution temperature, the CTA membrane was operated in PRO-mode, comprised of 32 g/L NaCl. Both the draw and the feed solutions were kept at a flow rate of 0.38 L/min (0.10 gpm), while the temperature of each solution is changed independently to 10, 20 and 30 °C for each experiment. In order to determine the effect of temperature on water flux across the membrane, experiments were also run in the presence of a temperature gradient but with deionized water on both sides of the membrane.

For these experiments, when the solution temperatures are different on either side of the membrane, there exists a temperature

**Table 3**
Water and salt permeabilities obtained from RO experiments.

| Parameter | Symbol (unit) | Feed concentration (g/L) | Temperature | | |
|---|---|---|---|---|---|
| | | | 10 | 20 | 30 |
| Pure water permeability | A (μm/s-MPa) | 0 | 1.95 ± 0.03 | 2.61 ± 0.10 | 3.14 ± 0.21 |
| Water permeability in presence of NaCl | $A_{NaCl\text{-}10}$ (μm/s-MPa) | 10 | | 2.56 ± 0.13 | |
| | $A_{NaCl\text{-}32}$ (μm/s-MPa) | 32 | 2.66 ± 0.11 | 2.96 ± 0.03 | 3.94 ± 0.76 |
| | $A_{NaCl\text{-}50}$ (μm/s-MPa) | 50 | | 3.67 ± 0.29 | |
| | $A_{NaCl\text{-}70}$ (μm/s-MPa) | 70 | | 4.91 ± 0.31 | |
| Intrinsic NaCl salt permeability | $B_{NaCl\text{-}10}$ ($10^{-7}$ m/s) | 10 | | 3.38 ± 0.57 | |
| | $B_{NaCl\text{-}32}$ ($10^{-7}$ m/s) | 32 | 3.24 ± 0.56 | 3.67 ± 0.80 | 4.66 ± 2.06 |
| | $B_{NaCl\text{-}50}$ ($10^{-7}$ m/s) | 50 | | 5.23 ± 1.01 | |
| | $B_{NaCl\text{-}70}$ ($10^{-7}$ m/s) | 70 | | 6.12 ± 0.48 | |
| Water permeability in presence of $MgSO_4$ | $A_{MgSO4}$ (μm/s-MPa) | 32 | | 2.75 ± 0.01 | |
| Intrinsic $MgSO_4$ salt permeability | $B_{MgSO4}$ ($10^{-7}$ m/s) | 32 | | 0.91 ± 0.11 | |
| Water permeability in presence of Instant Ocean | $A_{IO}$ (μm/s-MPa) | 32 | | 3.10 ± 0.16 | |
| Intrinsic Instant Ocean salt permeability | $B_{IO}$ ($10^{-7}$ m/s) | 32 | | 3.25 ± 0.31 | |

gradient within the membrane, which makes estimating the water and salt permeability difficult. From the data obtained from RO experiments in Table 3, we derived a best-fit correlation for water permeability as a function of temperature,

$$A(T) = \left(5.90 \times 10^{-14}\right)T + 1.38 \times 10^{-12} \quad (9)$$

where $A$ is measured in m/s-Pa and $T$ in °C. Similarly, a correlation for the NaCl salt permeability as a function of temperature was also obtained,

$$B(T) = \left(7.10 \times 10^{-9}\right)T + 2.44 \times 10^{-7} \quad (10)$$

where $B$ is in units of m/s.

Assuming a linear temperature gradient across the skin layer of the membrane, an average membrane temperature is used to estimate the average water and salt permeability coefficients using Eqs. (1) and (2). In doing so, consideration of the actual heat transfer at the surface of the membrane is implicitly neglected in these calculations.

*2.4.3. Variation of solution composition and chemistry*

The effects of solution composition and chemistry were studied when operated in PRO-mode with solution temperatures kept constant at 20 ± 1 °C, and flow rates kept constant at 0.38 L/min. Experiments were conducted with draw solution concentrations of 10, 32, 50 and 70 g/L NaCl, 32 g/L $MgSO_4$ and 32 g/L commercial sea salt (Instant Ocean).

*2.4.4. Variation of membrane orientation*

Finally, to evaluate how water flux changes with respect to membrane orientation, the membrane was tested in FO-mode with Milli-Q water as the feed, while the solution temperatures and flow rates were kept constant at 20 ± 1 °C, and 0.38 L/min, respectively. This membrane orientation was tested with draw solutions composed of 32 g/L NaCl, $MgSO_4$ and Instant Ocean.

## 3. Results and discussion

### 3.1. Membrane properties

From the RO experiments described in Section 2.2, pure water permeability, solution permeability, and salt permeability coefficients were obtained using Eqs. (1)–(3), supplemented with the physical–chemical data presented in Table 2. The resulting data is summarized in Table 3 and compares well with previously reported values [9,27]. The general trends are worth highlighting. As feed water temperature increases, water, solution, and salt permeability increase. In addition to changes in solvent, solute, and solution properties, the polymeric membrane expands upon heating producing larger effective pore sizes [40,41]. Salt permeability decreases as NaCl > Instant Ocean > $MgSO_4$, which scales with their respective diffusivities, and increases with higher salt concentration in the feed solution. As expected, the solution permeability corresponds with the salt permeability.

An important point to note is the appearance of the CTA membrane following RO compaction, as shown in Fig. 2. The membrane compacts over time at high applied pressures and develops long, thin "compression creases" along the length of the membrane, possibly indicating that the CTA membrane cannot support such high pressures and suffers irreversible inelastic strain as a result of the impact. Hence, water permeability coefficients determined for these membranes at high applied pressure do not represent the permeability in FO experiments where trans-membrane pressure is negligible. However, we expect all permeabilities in FO experiments to follow the general trends of values obtained in RO. Here, permeabilities were determined in RO only for applied pressures up to 400 psi where the values can be justified to reflect the membrane performance in FO experiments. The physical–chemical properties reported in Table 2 along with the $A$ and $B$ values reported in Table 3 were used to calculate the structural parameters for the FO experiments in which the solution chemistries, flow rates, and temperatures were varied.

**Table 4**
Average membrane parameters obtained from FO experiments using varying solution flow rates.

| Parameter | Units | Value |
|---|---|---|
| Apparent water permeability | μm/s-MPa | 2.20 ± 0.06 |
| Salt passage | μg/s | 5.61 ± 0.81 |
| Membrane structural parameter, $S$ | μm | 339 ± 30 |

### 3.2. Variation of solution flow rate

According to film theory, altering the solution flow rate changes the thickness of the mass transfer boundary layer at the surface of the membrane [42]. At higher flow rates, the boundary layer is thinner, which results in higher rate of mass transfer and, consequently, reduced concentration polarization. Table 4 presents the water permeability, salt passage and calculated structural parameters for CTA membranes tested under PRO-mode for different draw and feed solution flow rates. Neither water permeability nor salt passage varied significantly with the solution flow rate, indicating that external mass transfer played a minor role under the considered conditions.

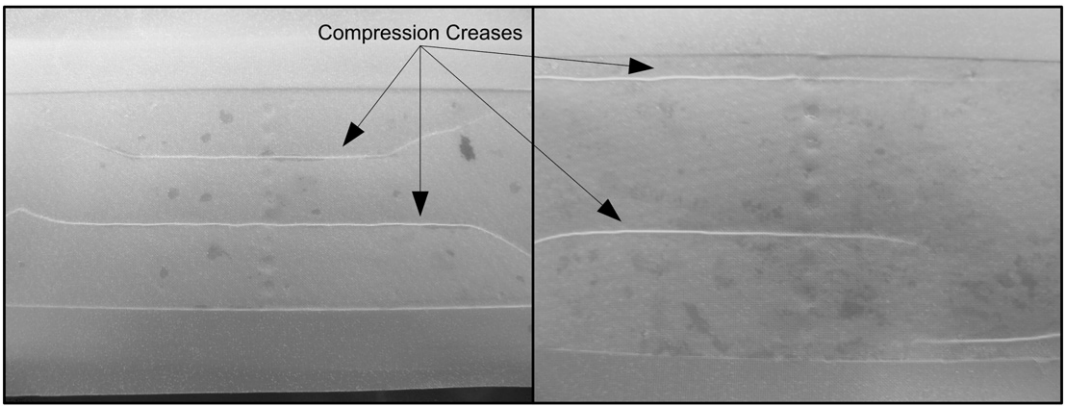


**Fig. 2.** CTA membrane after compaction at 400 psi under RO conditions showing compression creases along the length of the membrane.

As expected, the variations in the calculated structural parameter with the changes in flow rate are insignificant.

### 3.3. Variation of solution temperature

Thermo-osmosis, the transport of water through a semi-permeable membrane driven by a temperature gradient, has been considered previously for cellulose acetate membranes [43]. Experiments to test the influence of thermo-osmosis show that temperature gradients cause water fluxes an order of magnitude lower than that caused by a concentration gradient. These results are incorporated into the data obtained in the presence of a concentration gradient and are shown in Fig. 3, which shows that for a fixed draw solution temperature, increasing the feed solution temperature results in higher water permeability (Fig. 3A). Concurrently, the structural parameter decreases with the increase in draw solution temperature (Fig. 3B). These variations may be due to some thermally-induced changes of the membrane structure such as strain variations caused by different temperatures on each side of the membrane or weakening of intermolecular bonds within the cellulosic material. However, it may also be attributed to errors generated from the use of a constant-property theory; any errors inherent to simplifications made for the calculation are absorbed into the structural parameter. Certainly, a structural parameter of ~150 μm is not physical, but more likely a reflection of flaws in the theory used to interpret the experimental data. Specifically, changes in the water and salt permeability, which are mainly a function of the membrane skin layer will affect the structural parameter, which is intended to be characteristic of the porous substructure of the membrane as shown in Eqs. (1)–(4). Nevertheless, while such errors warrant caution in using the calculated parameters as strictly representative of their intended physical interpretation, the observed trends are most certainly indicative of some underlying processes which facilitate better mass transfer due to temperature gradients.

This sensitivity of the CTA membrane performance to solution temperature has important implications for its application. For example, where waste heat is available or where FO/PRO feed or draw streams are inherently at elevated temperatures, osmotic fluxes may be significantly enhanced; however, a trade-off may exist between high water flux and high salt rejection.

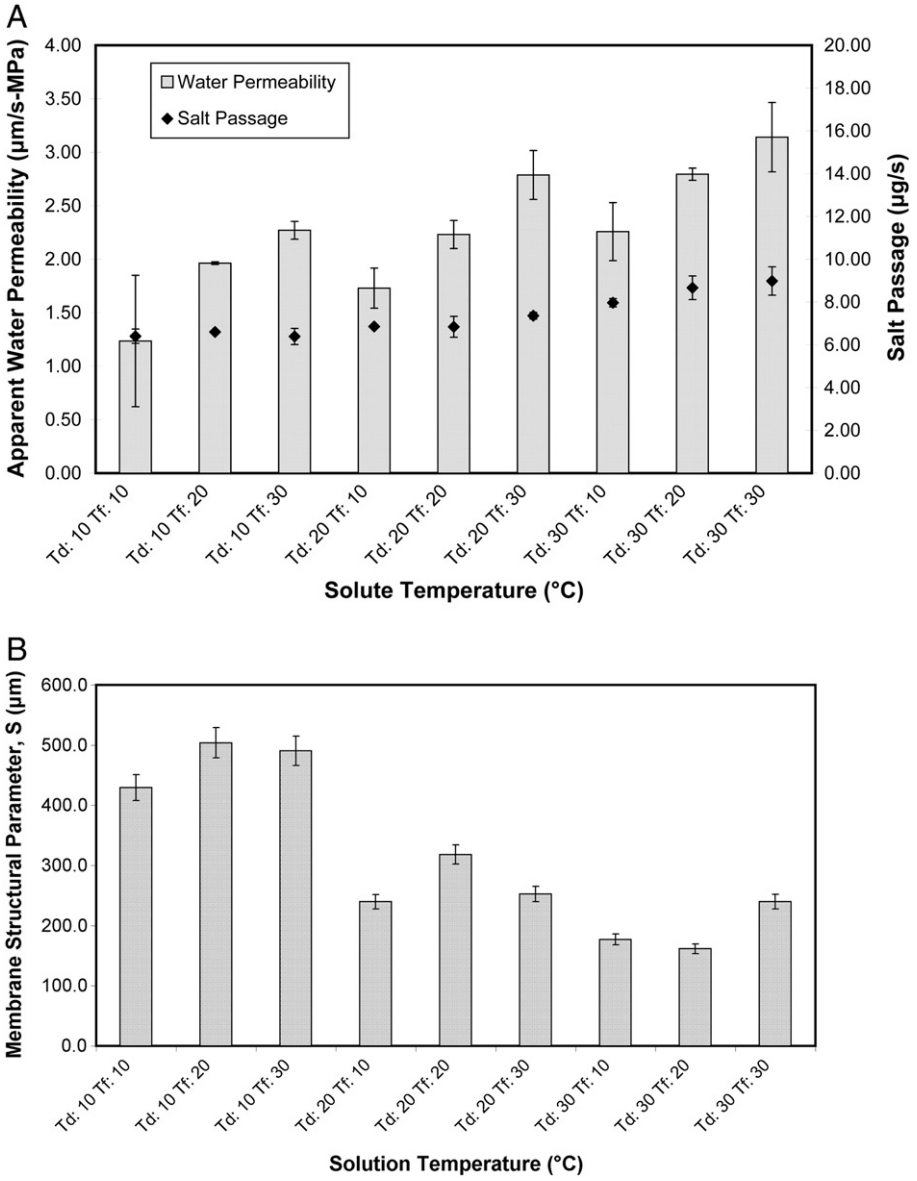


**Fig. 3.** Observed water and salt passage (A) and structural parameter (B) as a function of solution temperature in FO experiments.

### 3.4. Variation of solution concentration

As the concentration of NaCl in the draw solution increases, there is a slight decreasing trend in the apparent FO water permeability of the membrane (Fig. 4A). A similar observation has previously been reported by McCutcheon et al. [16]. The decrease in water permeability with increasing salt concentration has been attributed to osmotic de-swelling [44], in which case the salt permeability is also expected to decrease. However, in our experiments the salt permeation increased with draw solution concentration, which generally corresponds to a higher driving force for salt diffusion across the membrane. The structural parameter, calculated for draw solutions of 32, 50, and 70 g/L NaCl, was found to be relatively similar with an average value of about 300 μm (Fig. 4B). This value is slightly lower than the structural parameters previously reported for the CTA membrane operated in FO-mode [6,27]. Curiously, at a draw solution concentration of 10 g/L NaCl, the calculated structural parameter is significantly higher at ~500 μm. These results suggest that there are structural changes to the membrane in response to different salt concentrations. One possible explanation for the observed trends is the swelling of the cellulosic polymer in ionic solutions. The driving force for swelling is dependent on the difference between the charge density of the polymer and the ionic strength of the solution [18]. Therefore, at higher solution ionic strength, there is a greater ability of the solution to equalize the charge densities in the polymer, reducing electrostatic repulsion between polymer chains, and minimizing swelling [45]. This explains why the structural parameter was lower at the higher ionic strengths (32, 50, 70 g/L) and remains relatively constant, which may be indicative of maximal charge neutralization.

### 3.5. Variation of solution composition

The apparent water permeability in PRO-mode for different salt solutions is shown in Fig. 5A, with the following trend — NaCl > Instant Ocean > $MgSO_4$. On the other hand, the FO-mode water permeability does not significantly change with solution chemistry. Dilutive internal concentration polarization is expected to have a larger effect on water permeability compared with concentrative internal concentration polarization because the amount of salt that passes through the dense skin layer to concentrate the feed is much less than the

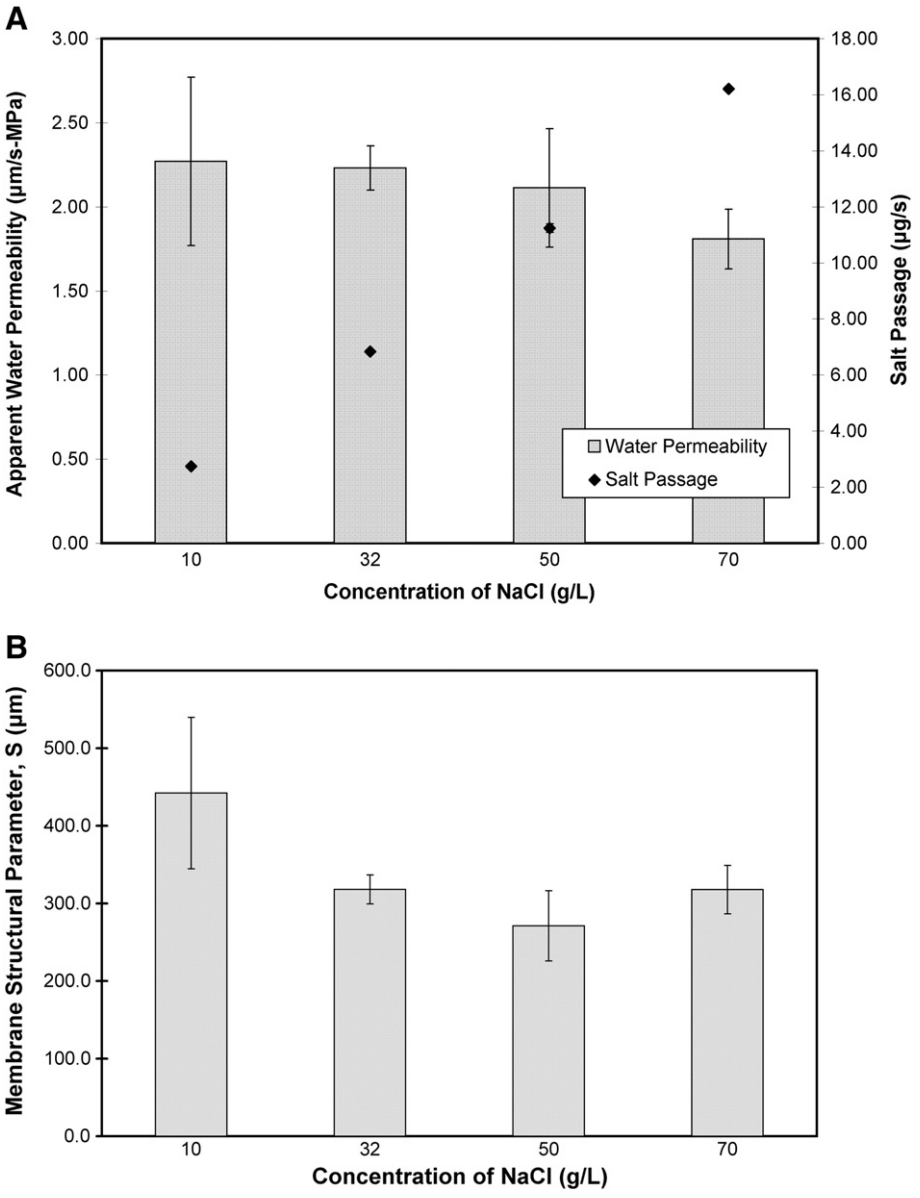


**Fig. 4.** Observed water and salt passage (A) and structural parameter (B) as a function of NaCl draw solution concentration in FO experiments.

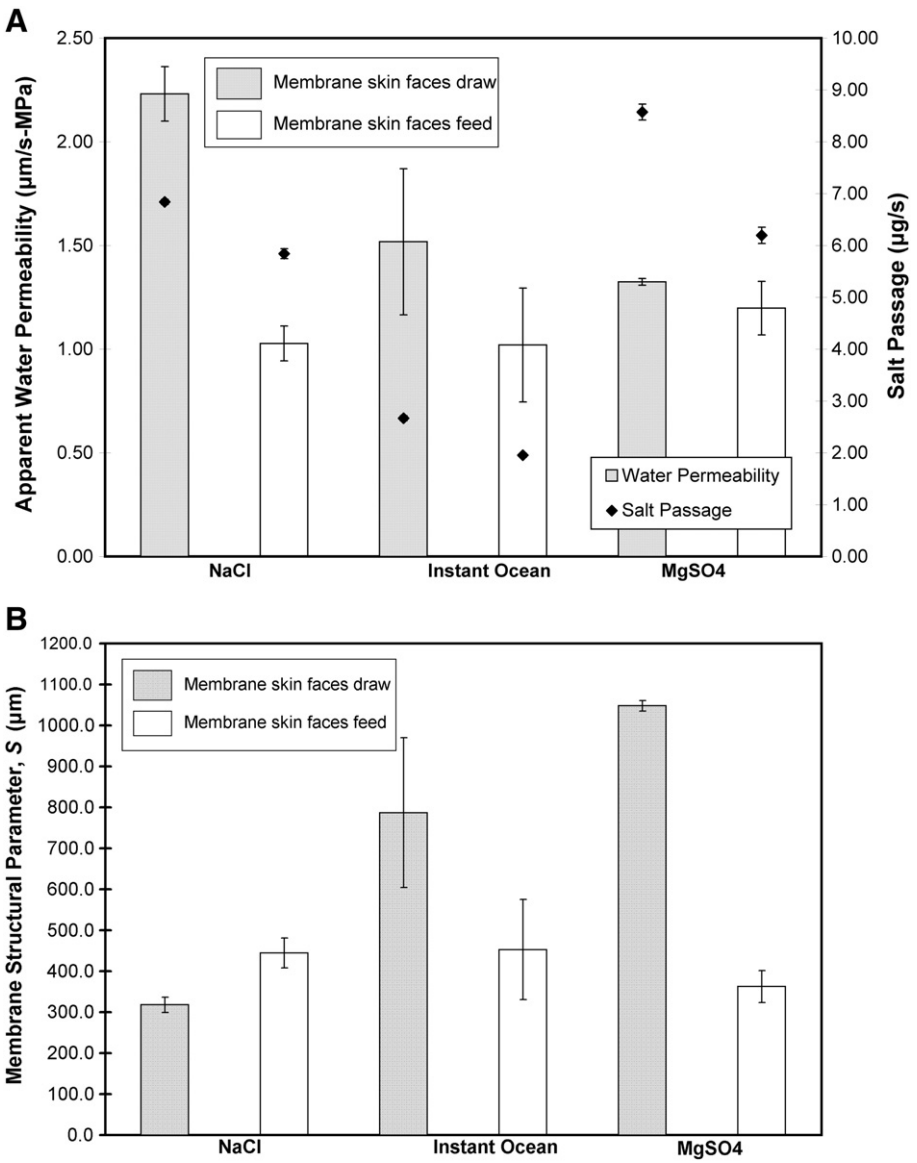


**Fig. 5.** Observed water and salt passage (A) and structural parameter (B) as a function of draw solution composition and membrane orientation in FO experiments.

amount of water that permeates through the porous support to dilute the draw as described in Section 2.3 [9]. Despite the greater loss of driving force, there are certainly important practical advantages to operate in FO-mode such as lower fouling propensity when the feed faces the smoother skin layer, and greater ease of cleaning the skin layer. PRO-mode is most suited for PRO processes to prevent delamination of the skin layer under pressurized draw solutions.

In PRO-mode, the calculated membrane structural parameter decreases as $MgSO_4$ > Instant Ocean > NaCl (Fig. 5B); meanwhile, in FO-mode the structural parameter does not significantly change with solution chemistry (consistent with the measured water permeability). The different salts may alter the membrane micro-void and, possibly, macro-void structure, to a varying extent. The concept of polymer swelling in response to contact with an ionic solution still applies in this case with regards to the salt permeability. In aqueous media, cations are highly hydrated, which, when incorporated into polymeric structures, will cause the polymer to swell [23]. Furthermore, salts interact electrostatically with the polymer matrix by neutralizing charge densities. Thus, divalent salts like $MgSO_4$ will possess a larger hydrated cation with an increased attraction to the partial negative charges on the acetate groups of the polymer. Instant Ocean has significant but less divalent cation content and NaCl is a 1:1 electrolyte. This means that the skin layer will swell to a greater extent in the presence of $MgSO_4$, causing it to be more swollen and less permeable, while the NaCl will cause the skin layer to be less swollen and more permeable.

Water permeability is predominantly a function of the skin layer structure, which in turn depends on the nature of the solution it is interacting with. However, the permeability of the skin layer is incorporated into the calculations of the membrane structural parameter (Eq. 4–6), which indicates that a more permeable membrane will inherently have a lower membrane structural parameter regardless of actual changes in the porous substructure. In FO-mode, the draw solution saturates the porous substructure, neutralizing the polymer charge densities, and causing swelling regardless of the salt solution used. This causes the structural parameter to be relatively similar for all the salts in FO-mode, as already reported in the literature [6]. As a final note, it should be re-iterated that while the observed experimental trends are certainly indicative of the effects imparted by salt composition, concentration and temperature, a full explanation

remains elusive; in particular, interpretation in terms of the structural parameter should be considered with caution, as the physically simplified model may not account for other mechanisms in effect.

## 4. Conclusions

In this study, experiments were carried out with the intent to probe the effects of flow rate, temperature and draw solution properties such as salinity and ionic composition on the performance of a commercially available CTA FO membrane. Particular attention was given to water permeability, salt passage and the calculated membrane structural parameter. Feed and draw solution flow rates did not significantly impact the measured water flux across the membrane, indicating that external mass transfer was not a limiting factor for the FO process. With increased temperature of either feed or draw solution, both the water permeability and salt passage increased, while the calculated structural parameter decreased; these effects may be explained by weakened molecular interactions in the polymeric membrane. As the draw solution ionic strength increased from brackish to seawater levels, the calculated structural parameter increased, presumably due to de-swelling of the polymer matrix; however, the small variability observed for higher salinities possibly indicates that the charge density was already completely neutralized. Solution chemistry (ionic composition) was observed to significantly impact the CTA membrane's permeability and the structural parameter, which again can be explained by swelling of the polymer matrix. The large changes in the structural parameter due to solution temperature, salinity, and composition explain at least some of the inter-laboratory variations in membrane properties reported in the literature to date. Finally, this study provides new insight into the possible mechanisms by which solution chemistry and process conditions conspire to govern the properties of osmotic membranes and their performance.

Supplementary materials related to this article can be found online at doi:10.1016/j.desal.2011.10.013.

*Nomenclature*

| | |
|---|---|
| $A$ | pure water permeability coefficient (m/s-Pa) |
| $A'(x)$ | water permeability in the presence of $x$ salt, where $x$ is NaCl, $MgSO_4$ or IO (Instant Ocean) (m/s-Pa) |
| $B_x$ | intrinsic salt permeability coefficient for $x$ salt (m/s) |
| $\Delta C$ | concentration difference across the skin layer of the membrane (g/L) |
| $C_{Db}$ | bulk draw solution concentration (g/L) |
| $C_{DECP}$ | reduced draw concentration at membrane surface due to external concentration polarization (g/L) |
| $C_{ICP}$ | concentration at internal surface of skin layer due to internal concentration polarization (g/L) |
| $C_{FECP}$ | reduced feed concentration at membrane surface due to external concentration polarization (g/L) |
| $C_{Fb}$ | bulk feed solution concentration (g/L) |
| $D$ | diffusion coefficient of solute in water ($m^2$/s) |
| $d_H$ | hydraulic diameter (m) |
| $J_w$ | water flux across the membrane (m/s) |
| $K$ | resistance to solute diffusion in the porous support of the membrane (m/s) |
| $k$ | mass transfer coefficient (m/s) |
| $\Delta P$ | applied hydraulic pressure (Pa) |
| $\Delta\pi_{eff}$ | effective osmotic pressure difference (Pa) |
| $\Delta\pi_{bulk}$ | bulk osmotic pressure difference (Pa) |
| $Q$ | volumetric flow rate ($m^3$/s or gpm) |
| $R$ | solute rejection |
| $Re$ | Reynolds number $= (u_0\rho d_H)/\mu$ |
| $S$ | membrane structural parameter (m) |
| $Sc$ | Schmidt number $= \mu/(\rho D)$ |
| $Sh$ | Sherwood number $= kd_H/D$ |
| $u_0$ | crossflow velocity (m/s) |
| $T_d$ | temperature of the draw solution (°C) |
| $T_f$ | temperature of the feed solution (°C) |
| $t_{sup}$ | thickness of porous support layer (m) |

*Greek letters*

| | |
|---|---|
| $\varepsilon$ | porosity of porous support |
| $\tau$ | tortuosity of porous support |

## Acknowledgments

The work presented in this publication was supported by Award No. KUS-C1-018-02, made by King Abdullah University of Science and Technology (KAUST). GZR was supported by a Vaadia-BARD Postdoctoral Fellowship Award No. FI-435-2010 from BARD, The United States–Israel Binational Agricultural Research and Development Fund.

## References

[1] B. Kingsolver, B. Larmer, T. Pankratz, Water: our thirsty world, National Geographic, A Special Issue, National Geographic Society, New York, NY, 2010.
[2] M. Elimelech, The global challenge for adequate and safe water, Journal of Water Supply Research and Technology-AQUA 55 (2006) 3–10.
[3] G.M. Geise, H.-S. Lee, D.J. Miller, B.D. Freeman, J.E. McGrath, D.R. Paul, Water purification by membranes: the role of polymer science, J. Polym. Sci., Part B: Polym. Phys. 48 (2010) 1685–1718.
[4] M. Elimelech, W.A. Phillip, The future of seawater desalination: energy, technology, and the environment, Science 333 (2011) 712–717.
[5] T. Pankratz, The big idea, National Geographic, National Geographic Society, New York, NY, 2010 32-36.
[6] A. Achilli, T.Y. Cath, A.E. Childress, Selection of inorganic-based draw solutions for forward osmosis applications, J. Membr. Sci. 364 (2010) 233–241.
[7] A. Tiraferri, N.Y. Yip, W.A. Phillip, J.D. Schiffman, M. Elimelech, Relating performance of thin-film composite forward osmosis membranes to support layer formation and structure, J. Membr. Sci. 367 (2011) 340–352.
[8] J.E. Miller, L.R. Evans, Forward Osmosis: A New Approach to Water Purification and Desalination, Sandia National Laboratories, Albuquerque, NM, 2006.
[9] T.Y. Cath, A.E. Childress, M. Elimelech, Forward osmosis: principles, applications and recent developments, J. Membr. Sci. 281 (2006) 70–87.
[10] Q. Yang, K.Y. Wang, T.-S. Chung, A novel dual-layer forward osmosis membrane for protein enrichment and concentration, Sep. Purif. Technol. 69 (2009) 269–274.
[11] E.M. Garcia-Castello, J.R. McCutcheon, M. Elimelech, Performance evaluation of sucrose concentration using forward osmosis, J. Membr. Sci. 338 (2009) 61–66.
[12] K.L. Lee, R.W. Baker, H.K. Lonsdale, Membranes for power generation by pressure-retarded osmosis, J. Membr. Sci. 8 (1981) 141–171.
[13] S. Loeb, Production of energy from concentrated brines by pressure-retarded osmosis: 1. Preliminary technical and economic considerations, Journal of Membrane Science 1 (1976) 49–63.
[14] S. Loeb, Large-scale power production by pressure-retarded osmosis, using river water and sea water passing through spiral modules, Desalination 143 (2002) 115–122.
[15] T. Thorsen, T. Holt, The potential for power production from salinity gradients by pressure retarded osmosis, J. Membr. Sci. 335 (2009) 103–110.
[16] J.R. McCutcheon, R.L. McGinnis, M. Elimelech, Desalination by ammonia–carbon dioxide forward osmosis: influence of draw and feed solution concentrations on process performance, J. Membr. Sci. 278 (2006) 114–123.
[17] G.T. Gray, J.R. McCutcheon, M. Elimelech, Internal concentration polarization in forward osmosis: role of membrane orientation, Desalination 197 (2006) 1–8.
[18] M.F. McCurley, W.R. Seitz, Fiber-optic sensor for salt concentration based on polymer swelling coupled to optical displacement, Anal. Chim. Acta 249 (1991) 373–380.
[19] H. Muta, M. Miwa, M. Satoh, Ion-specific swelling of hydrophilic polymer gels, Polymer 42 (2001) 6313–6316.
[20] D.J. Buckley, M. Berger, The swelling of polymer systems in solvents. II. Mathematics of diffusion, Journal of Polymer Science 56 (1962) 175–188.
[21] W.R. Moore, J. Russell, Swelling and absorption by cellulose acetate in binary solvent–hexane mixtures, Journal of Polymer Science 18 (1955) 63–89.
[22] A.E. Alexander, B. Rabinovitch, The Swelling and Solubility of Cellulose Acetate in Benzene/Xylenol Mixtures, The Royal Society, London, 1950, pp. 154–162.
[23] R.E. Kesting, Semipermeable membranes of cellulose acetate for desalination in the process of reverse osmosis. I. Lyotropic swelling of secondary cellulose acetate, J. Appl. Polym. Sci. 9 (1965) 663–668.
[24] J. McMurry, Biomolecules: Carbohydrates, Organic Chemistry, Thomson Learning, Belmont, CA, 2004.
[25] J.R. McCutcheon, M. Elimelech, Influence of membrane support layer hydrophobicity on water flux in osmotically driven membrane processes, J. Membr. Sci. 318 (2008) 458–466.
[26] H.K. Lonsdale, U. Merten, R.L. Riley, Transport properties of cellulose acetate osmotic membranes, J. Appl. Polym. Sci. 9 (1965) 1341–1362.

[27] N.Y. Yip, A. Tiraferri, W.A. Phillip, J.D. Schiffman, M. Elimelech, High performance thin-film composite forward osmosis membrane, Environ. Sci. Technol. 44 (2010) 3812–3818.
[28] M.L. Lind, B.H. Jeong, A. Subramani, X.F. Huang, E.M.V. Hoek, Effect of mobile cation on zeolite–polyamide thin film nanocomposite membranes, Journal of Materials Research 24 (2009) 1624–1631.
[29] A.K. Ghosh, E.M.V. Hoek, Impacts of support membrane structure and chemistry on polyamide–polysulfone interfacial composite membranes, J. Membr. Sci. 336 (2009) 140–148.
[30] C.P. Koutsou, S.G. Yiantsios, A.J. Karabelas, A numerical and experimental study of mass transfer in spacer-filled channels: effects of spacer geometrical characteristics and Schmidt number, J. Membr. Sci. 326 (2009) 234–251.
[31] G. Guillen, E.M.V. Hoek, Modeling the impacts of feed spacer geometry on reverse osmosis and nanofiltration processes, Chem. Eng. J. 149 (2009) 221–231.
[32] G. Shock, A. Miguel, Mass transfer and pressure loss in spiral wound modules, Desalination 64 (1987) 339–352.
[33] F.J. Millero, A. Poison, International one-atmosphere equation of state of seawater, Deep Sea Research 28A (1981) 625–629.
[34] Concentrative properties of aqueous solutions: density, refractive index, freezing point depression, and viscosity, in: D.R. Lide (Ed.), Handbook of Chemistry and Physics, 2011.
[35] V.M. Lobo, Mutual diffusion coefficients in aqueous electrolyte solutions, Pure Appl. Chem. 65 (1993) 2613–2640.
[36] J.T. Edward, Molecular volumes and the Stokes–Einstein equation, J. Chem. Educ. 47 (1970) 261–270.
[37] S. Loeb, T. Leonid, E. Korngold, J. Freiman, Effect of porous support fabric on osmosis through a Loeb–Sourirajan type asymmetric membrane, J. Membr. Sci. 129 (1997) 243–249.
[38] J.C. Crittenden, R.R. Trussell, D.W. Hand, K.J. Howe, G. Tchobanoglous, Reverse osmosis, Water Treatment: Principles and Design, John Wiley & Sons, Hoboken, New Jersey, 2005, pp. 1429–1506.
[39] N.Y. Yip, A. Tiraferri, W.A. Phillip, J.D. Schiffman, L.A. Hoover, Y.C. Kim, M. Elimelech, Thin-film composite pressure retarded osmosis membranes for sustainable power generation from salinity gradients, Environ. Sci. Technol. 45 (2011) 4360–4369.
[40] A. Jawor, E.M.V. Hoek, Effects of feed water temperature on inorganic fouling of brackish water RO membranes, Desalination 235 (2009) 44–57.
[41] X. Jin, X.F. Huang, E.M.V. Hoek, Role of specific ion interactions in seawater RO membrane fouling by alginic acid, Environ. Sci. Technol. 43 (2009) 3580–3587.
[42] C.J. Geankoplis, Principles of Mass Transfer, Transport Processes and Separation Process Principles, Prentice Hall, Upper Saddle River, NJ, 2003, pp. 410–456.
[43] M.S. Dariel, O. Kedem, Thermoosmosis in semipermeable membranes, J. Phys. Chem. 79 (1975) 336–342.
[44] G.D. Mehta, S. Loeb, Performance of permasep B-9 and B-10 membranes in various osmotic regions and at high osmotic pressures, J. Membr. Sci. 4 (1978) 335–349.
[45] P.J. Flory, Principles of Polymer Chemistry, Cornell University Press, Ithaca, NY, 1953.